THE JOURNAL OF PHYSICAL CHEMISTRY C

Article

pubs.acs.org/JPCC

Analysis of Molecular Clusters in Simulations of Lithium-Ion Battery Electrolytes

Craig M. Tenney* and Randall T. Cygan

Sandia National Laboratories, Albuquerque, New Mexico, 87123 United States

Supporting Information

ABSTRACT: Graph theoretic tools were used to identify and classify clusters of ions and solvent molecules in molecular dynamics simulations of lithium-ion battery electrolytes. Electrolytes composed of various concentrations of $LiPF_6$ dissolved in ethylene carbonate (EC), dimethylene carbonate (DMC), or a 1:1 EC/DMC mixture were simulated at multiple temperatures using classical molecular dynamics. Contrary to Nernst−Einstein theory but consistent with experiment, pure DMC systems had the greatest diffusivity but the lowest conductivity. This disagreement with Nernst−Einstein theory is explained by the observed clustering behavior, which found that systems with pure EC as a solvent formed ion clusters with nonzero charge, whereas systems with pure DMC as a solvent formed primarily neutral clusters.

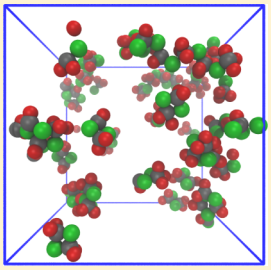

INTRODUCTION

Understanding the behavior of liquid electrolytes for lithium-ion secondary batteries is important for improving the performance of portable electronics devices, electric vehicles, and hybrid electric vehicles and can ultimately impact the development of new energy storage technologies.[1,2] The transport of Li^+ through an electrolyte is critical for determining the rate of energy release during operation of a rechargeable battery. Transport of charge by Li^+ between electrodes requires an efficient process that is not jeopardized by chemical reactions or strong molecular associations that impede the diffusion of Li^+ over multiple cycles of battery operation. Practical electrolyte materials require electrochemical stability, have high ionic conductivity, and should be good electronic insulators to ensure optimal battery performance.[3]

Polar organic solvents such as ethylene carbonate (EC) and dimethyl carbonate (DMC) are commonly used as electrolytes in lithium secondary batteries. In addition, binary and multicomponent mixtures of such solvents have been helpful in improving electrolyte behavior at various temperatures and in optimizing physical and electrochemical properties.[4] Cyclic esters such as EC are characterized by high dielectric constants ($\epsilon = 90$ for EC) and are relatively viscous ($\eta = 2$ cP for EC), while acyclic esters are weakly polar ($\epsilon = 4$ for DMC) and more fluid ($\eta = 0.6$ cP for DMC).[3] This contrast in bulk physical properties is attributed to molecular conformations involving the alignment of relatively planar and compact EC molecules and their dipoles compared to those for the more flexible structure associated with linear and open DMC molecules that lead to a bulk cancellation of their dipoles. Based on chemical and physical properties, lithium hexafluorophosphate salt ($LiPF_6$) is the predominant solute for nonaqueous electrolytes in lithium batteries. $LiPF_6$ salt in organic carbonate solvents has a large dissociation into its component ions, which, having high ionic mobility, results in an excellent ionic conductivity for the electrolyte.

Experimental and spectroscopic studies of polar organic electrolytes include a wide range of techniques to evaluate the structure and dynamics of Li^+, salt, and solvent molecules. These include neutron and X-ray diffraction, vibrational spectroscopy, X-ray photoelectron spectroscopy, X-ray and neutron scattering, nuclear magnetic resonance, and other methods.[5−10] Along with traditional electrical conductivity measurements, these methods provide significant insight into the molecular mechanisms associated with Li^+ transport and complex interactions of the coordinating solvent molecules. Additionally, advances in both computational chemistry methods and high performance computing platforms have led to the development of improved predictive molecular models of many types of materials, including battery components.[11,12]

Although classical molecular simulations of electrolyte structure and dynamics have been effectively utilized by several research groups to evaluate Li^+ diffusion in organic solvents,[8,13−17] there remain several questions regarding relative diffusion rates, concentration effects, and the coordination environment of Li^+, especially for comparison of pure and mixed solvents at various salt concentrations and temperatures. Recent modeling studies of lithium dynamics in EC electrolyte using ab initio methods and density functional theory avoid the need for an empirical-based forcefield but are, at present, limited by accuracy of the energy density functionals and by large computational cost even for simulations of a few tens of solvent molecules.[18,19]

In this study, we employ a relatively simple set of interatomic potentials to describe the bonded and nonbonded interactions between atoms for simulation cells possessing a thousand solvent molecules and tens of Li−PF_6 pairs. Molecular dynamics (MD) simulations are used to derive equilibrated electrolyte structures, and resulting atomic trajectories are employed to examine structure and transport properties. Finally, graph theory and cluster

Received: April 19, 2013
Revised: October 21, 2013
Published: October 23, 2013

   dx.doi.org/10.1021/jp4039122 | J. Phys. Chem. C 2013, 117, 24673−24684

topologies are used to better evaluate the significance of cluster size, composition, and charge on diffusion and conductivity.

SIMULATION DETAILS

Molecular dynamics (MD) was used to study the properties of lithium-ion battery electrolytes composed of nonaqueous solvent (ethylene carbonate (EC) and/or dimethyl carbonate (DMC)) with $LiPF_6$ salt. Figure 1 shows the minimum energy

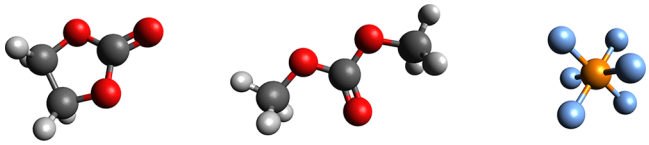

(a) EC (b) DMC (c) PF_6^-

Figure 1. Structures of solvent and ion species used in this study (except lithium cation (Li^+)): ethylene carbonate (EC), dimethyl carbonate (DMC), hexafluorophosphate (PF^{-6}). (carbon = grey, oxygen = red, hydrogen = white, phosphorous = orange, fluorine = light blue)

(B3LYP/aug-cc-pvdz, vacuum) structures of EC, DMC, and PF_6^-. MD simulations were performed for all combinations of three temperatures (300, 350, and 400 K), three solvent compositions (pure EC, pure DMC, and 1:1 EC/DMC), and three $LiPF_6$ concentrations (approximately 0.1, 0.3, and 1.0 M), i.e., a total of 27 temperature/solvent/concentration combinations. The pressure for each simulation was set to 1.0 atm. A total of 1000 solvent molecules was used in each simulation. The number of Li-PF6 ion pairs in each simulation was 8, 24, or 75.

A simple "Class I" force field model was used to describe bonded and nonbonded interactions between atoms:

$$E_{\text{total}} = \sum_{\text{bonds}} K_r(r - r_0)^2 + \sum_{\text{angles}} K_\theta(\theta - \theta_0)^2 + \sum_{\text{dihedrals}} K_{\phi,n}[1 + \cos(n\phi - \gamma)] + \sum_{i<j} 4\epsilon_{i,j}\left[\left(\frac{\sigma_{ij}}{r_{ij}}\right)^{12} - \left(\frac{\sigma_{ij}}{r_{ij}}\right)^{6}\right] + \sum_{i<j}\frac{q_i q_j}{r_{ij}} \quad (1)$$

The bonded interaction parameters K_r, K_θ, and $K_{\phi,n}$ are force constants; r_0 is equilibrium bond length; θ_0 is equilibrium bond angle; and n and γ are periodicity and phase angle, respectively, for dihedral interactions. Note that the summation over dihedral bonds includes both conventional and "improper" dihedrals. Accounting for nonbonded contributions to the potential energy, the Lennard-Jones parameters ϵ and σ describe repulsive and dispersive interactions, and the point charges q describe electrostatic interactions. For Lennard-Jones interactions between different atom types, parameters $\epsilon_{i,j}$ and $\sigma_{i,j}$ were calculated using Lorentz−Berthelot combining rules:

$$\epsilon_{i,j} = \sqrt{\epsilon_{i,i}\epsilon_{j,j}}\,\sigma_{i,j} = \frac{\sigma_{i,i} + \sigma_{j,j}}{2} \quad (2)$$

Intramolecular nonbonded interactions between atoms separated by one or two bonds ("1−2" and "1−3" interactions) were set to zero. Intramolecular Lennard-Jones and electrostatic pairwise interactions between atoms separated by three bonds ("1−4" interactions) were scaled by 0.5 and 0.8333, respectively. Intramolecular nonbonded interactions between atoms separated by more than three bonds were unscaled.

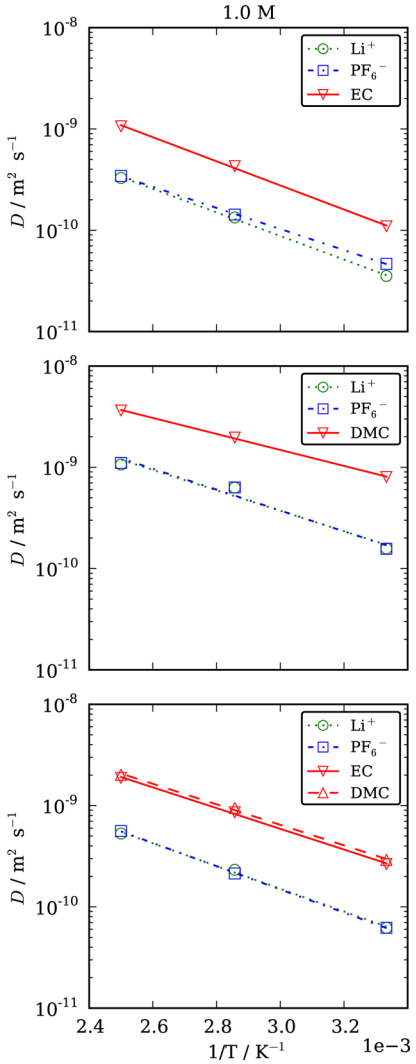

Figure 2. Ion and solvent self-diffusion coefficients D (eq 4) versus $1/T$ for 1.0 M $LiPF_6$ in EC (top), DMC (middle), and EC/DMC (bottom) solvents. Values for D are averages taken over the last 8 ns of 20 ns trajectories. Symbol sizes are approximately equivalent to two standard deviations. Lines are regression fits to eq 5

Table 1. Arrhenius Activation Energies E (in Degrees K, See eq 5) Associated with the Diffusion of Ions and Solvent Molecules for the Systems Described in Figure 2[a]

	Li^+	PF_6^-	EC	DMC
EC	2600	2400	2750	
DMC	2300	2300		1820
EC/DMC	2500	2600	2360	2340

[a]Uncertainties in E are approximately 100 K for Li^+ and PF_6^- and approximately 10 K for EC and DMC.

The functional form of the force field used in this study does not explicitly model atomic polarizability. While the increased degrees of freedom in polarizable force fields (e.g., refs 15 and 20) can improve quantitative accuracy over a wider range of conditions, especially for ionic systems such as this, the greater resources required to use such a force field were not justified by the goals of this study.

Force field parameters for lithium ion were taken from the OPLS force field.[21] To develop force fields for EC, DMC, and PF_6^-, an energy-minimized ab initio structure was first generated

dx.doi.org/10.1021/jp4039122 | J. Phys. Chem. C 2013, 117, 24673−24684

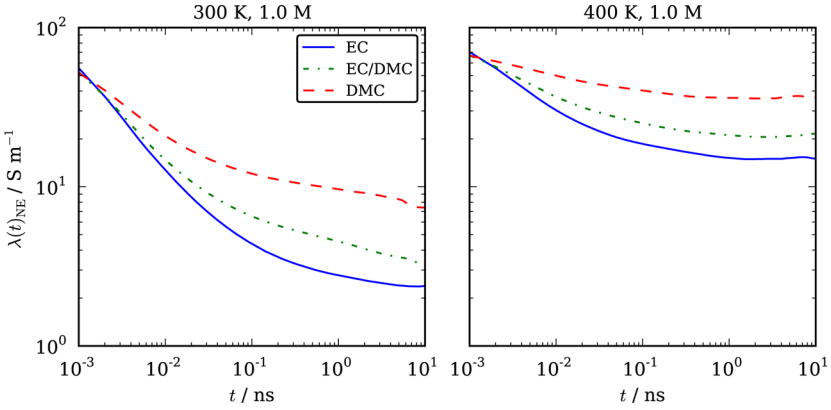

Figure 3. Theoretical Nernst−Einstein (uncorrelated) ionic conductivity $\lambda_{NE}(t)$ ($i = j$ diagonal terms of eq 6) versus time t for 1.0 M $LiPF_6$ in EC, DMC, and EC/DMC solvents at 300 and 400 K.

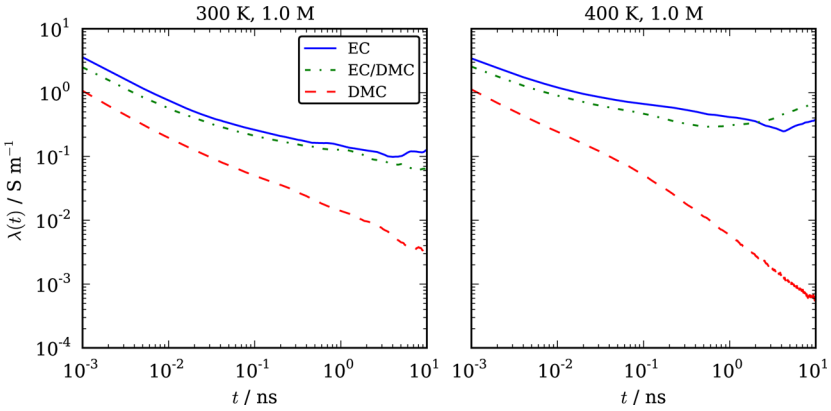

Figure 4. As in Figure 3, except true (correlated) ionic conductivity $\lambda(t)$ (eq 6).

using Gaussian 03[22] at the B3LYP/aug-cc-pvdz level of theory. From the results of this calculation, the open source Antechamber[23] suite of force field tools was used to assign initial bonded and nonbonded force field parameters from the generalized AMBER force field (GAFF).[24] Also during this step, atomic point charges were calculated from the ab initio results via Antechamber using the restrained electrostatic potential (RESP)[25,26] method. After initial assignment of parameters via Antechamber, the resulting force field for a given molecule was refined, if necessary, by assigning different GAFF atom types in order to yield a pattern of bond types more consistent with ab initio results. Lennard-Jones, bond, angle, and dihedral parameters for the various atom types were not changed from their GAFF values. Specific values for the force field parameters used in this work can be found in the Supporting Information.

Using the force fields described above, all MD simulations were conducted using the open-source LAMMPS (version 19 Jul 2011) MD code.[27,28] Example LAMMPS input scripts demonstrating specific simulation settings are provided in the Supporting Information.

For a given combination of solvent composition and salt concentration, an initial low-density system was constructed by randomly placing the required molecules into a cube using the open-source simulation setup tool Packmol[29] and then compressing the system to a density close to experimental values over 0.1 ns at 300K. Subsequent isothermal−isobaric (NPT) simulations were started from these initial systems. Total NPT simulation time was 10−20 ns. The first 1 ns of data was discarded from each simulation to allow systems to relax. For the systems with the slowest dynamics (i.e., 300 K and pure EC), system volume and energies were oscillating about their long-term averages after 0.5 ns.

System trajectory snapshots were recorded every 1 ps. These trajectories were postprocessed to calculate mean-squared displacements, diffusivities, conductivities, pair correlation functions, coordination numbers, pair autocorrelation functions, and cluster network topologies for each of the 27 systems described previously.

RESULTS AND DISCUSSION

Diffusivity. The mean-square displacement (MSD) of the center of mass of a set of N molecules during time t is

$$\mathrm{MSD}(t) = \frac{1}{N}\sum_{i}^{N} \langle [\mathbf{r}_i(t_0 + t) - \mathbf{r}_i(t_0)]^2 \rangle \tag{3}$$

where $\mathbf{r}_i(\tau)$ is the position of molecule i at time τ and $\langle\rangle$ denotes an ensemble average over possible starting times t_0. The self-diffusion coefficient D for a species i can be calculated from eq 3 using the Einstein relation

$$D_i = \lim_{t\to\infty} \frac{\mathrm{MSD}_i(t)}{6t} \tag{4}$$

Figure 2 shows ion and solvent molecule self-diffusion coefficients D (eq 4) versus inverse temperature $1/T$ for 1.0 M $LiPF_6$ in EC, DMC, and EC/DMC solvents at 300, 350, and 400 K. Solvent diffusivities are significantly higher in pure DMC systems than in pure EC systems, particularly at 300 K.

dx.doi.org/10.1021/jp4039122 | J. Phys. Chem. C 2013, 117, 24673−24684

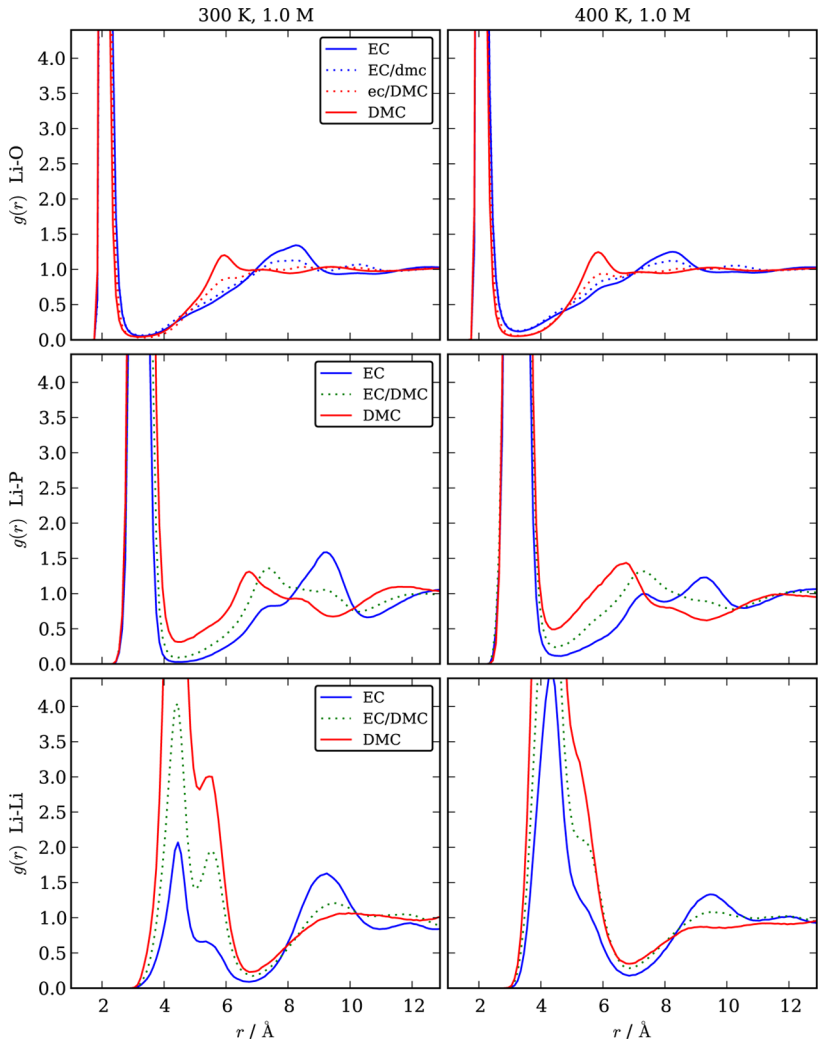

Figure 5. Pair correlation functions $g(r)$ versus separation r for Li^+ with solvent carbonyl oxygens (Li−O), PF_6^- (Li−P), and other Li^+ (Li−Li) for 1.0 M $LiPF_6$ in EC, DMC, and EC/DMC solvents at 300 and 400 K. "EC/dmc" and "ec/DMC" denote Li−O coordination of Li^+ with EC and DMC, respectively, in mixed EC/DMC solvent systems.

Table 2. Average Number of Solvent Carbonyl Oxygen Atoms within First Coordination Shell of Li^+ for All Combinations of Solvent, Temperature, and $LiPF_6$ Concentration Used in This Study[a]

	0.1 M $LiPF_6$			0.3 M $LiPF_6$			1.0 M $LiPF_6$		
	300 K	350 K	400 K	300 K	350 K	400 K	300 K	350 K	400 K
EC	5.2	5.0	4.2	5.1	4.2	3.6	4.0	3.3	2.9
EC/dmc	3.0	2.4	2.0	2.5	1.8	1.6	1.6	1.5	1.3
ec/DMC	2.0	1.6	1.4	1.8	1.5	1.3	1.6	1.4	1.2
DMC	2.6	2.1	2.1	2.5	2.1	2.0	2.3	2.0	2.0

[a]"EC/dmc" and "ec/DMC" denote coordination of Li^+ with EC and DMC, respectively, in mixed EC/DMC solvent systems.

This trend is consistent with the high viscosity and melting point of EC, relative to DMC.[3] In mixed EC/DMC systems, DMC and EC diffusivities are nearly identical and approximately equal to the average of values observed in corresponding pure DMC and EC systems. Solvent diffusivities are 2−5× larger than ion diffusivities for any particular system, which would be consistent with the formation of bulky, slowly diffusing molecular clusters associated with the ions. Variations in ion diffusivity between different systems match the trends observed for variations in solvent diffusivity, which is consistent with the Stokes−Einstein relation and with experimental observations that show solvent and ion diffusivities are inversely proportional to solution viscosity.[30] For EC and EC/DMC systems at lower $LiPF_6$ concentrations (not shown), PF_6^- diffusivities appear to be slighter greater than those for Li^+. Decreasing $LiPF_6$ concentration to 0.1 M (not shown) leads to increased diffusivities for all species, which would be consistent with decreased cluster formation and reduced system viscosity. This effect is relatively slight for the pure DMC systems (1.2×) but significant for pure EC systems (3× at 300 K and 1.7× at 400 K), suggesting that EC and DMC may interact fundamentally differently with the Li^+ and/or PF_6^- ions present in the system. For systems composed of 1.0 M $LiPF_6$ in EC at 300 and 350 K, self-diffusion coefficients from simulation are approximately 50% of

dx.doi.org/10.1021/jp4039122 | J. Phys. Chem. C 2013, 117, 24673−24684

Table 3. As in Table 2, except for Coordination of PF_6^- Ions with Li^+

	0.1 M $LiPF_6$			0.3 M $LiPF_6$			1.0 M $LiPF_6$		
	300 K	350 K	400 K	300 K	350 K	400 K	300 K	350 K	400 K
EC	0.4	0.4	0.8	0.4	0.9	1.1	1.1	1.4	1.6
EC/DMC	0.5	0.9	1.2	0.8	1.4	1.6	1.5	1.7	1.9
DMC	1.7	2.0	2.0	1.9	2.1	2.2	2.1	2.2	2.2

Table 4. As in Table 2, except for Coordination of Li^+ Ions with Li^+

	0.1 M $LiPF_6$			0.3 M $LiPF_6$			1.0 M $LiPF_6$		
	300 K	350 K	400 K	300 K	350 K	400 K	300 K	350 K	400 K
EC	0.0	0.0	0.1	0.0	0.3	0.5	0.4	0.7	0.9
EC/DMC	0.0	0.2	0.3	0.1	0.6	0.7	0.9	1.1	1.3
DMC	0.9	1.0	1.0	1.4	1.4	1.6	1.6	1.6	1.7

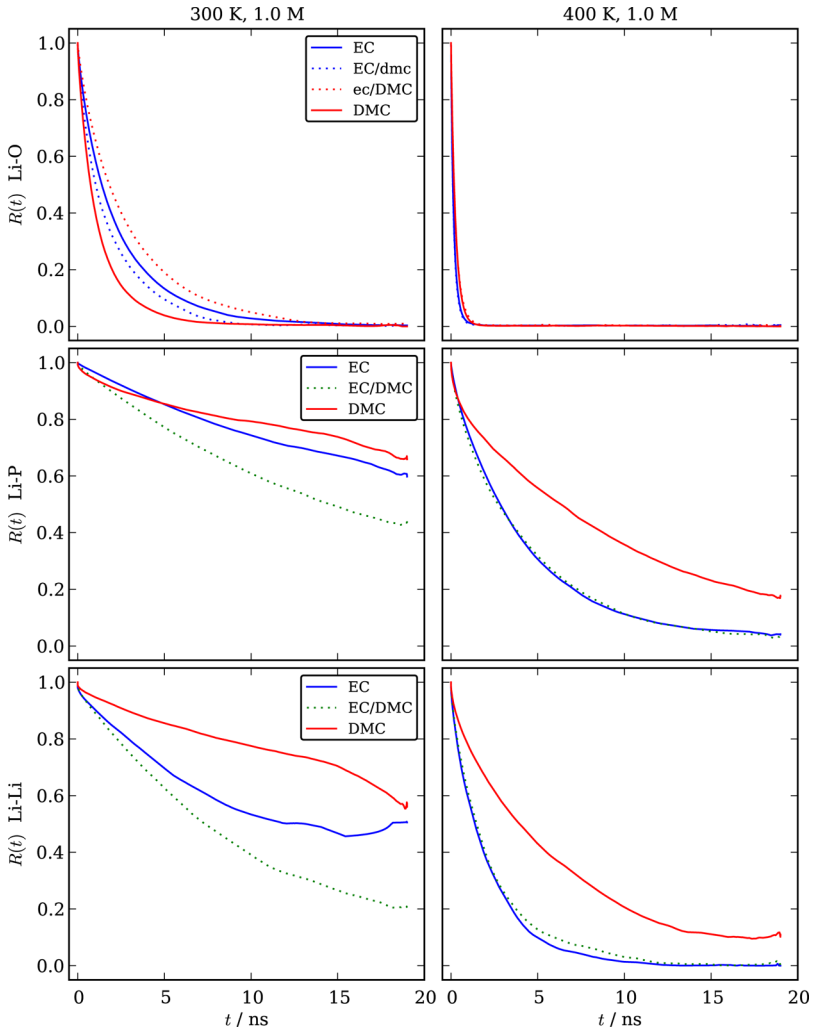

Figure 6. Neighbor autocorrelation function $R(t)$ (eq 9) versus time t for Li^+ with solvent carbonyl oxygens (Li−O), PF_6^- (Li−P), and other Li^+ (Li−Li) for 1.0 M $LiPF_6$ in EC, DMC, and EC/DMC solvents at 300 and 400 K. A "neighbor" is defined as an atom closer than the minimum after the first peak of the corresponding $g(r)$ in Figure 5.

experimentally observed values for EC, 25% for PF_6^-, and 30% for Li^+.[31]

Activation energies E associated with the diffusion of ions and solvent molecules were calculated for the systems represented in Figure 2 by fitting the data to an Arrhenius expression

$$D = D_\infty e^{-E/T} \quad (5)$$

where D_∞ is the limiting value of D extrapolated to $T = \infty$. The resulting values of E are summarized in Table 1. Activation energies for diffusion of Li^+ and PF_6^- are similar and do not appear to vary greatly between the three choices of solvent. Values of E for solvent diffusion do, however, vary strongly with solvent choice. Specifically, solvent diffusion depends more strongly upon temperature in pure EC systems than in pure DMC systems,

dx.doi.org/10.1021/jp4039122 | J. Phys. Chem. C 2013, 117, 24673−24684

with mixed EC/DMC systems displaying intermediate temperature dependence.

Ionic Conductivity. Ionic conductivity λ can be calculated using the Einstein relation

$$\lambda(t) = \frac{e^2}{6tVk_BT}\sum_i^N\sum_j^N z_i z_j\langle[\mathbf{r}_i(t_0+t) - \mathbf{r}_i(t_0)][\mathbf{r}_j(t_0+t) - \mathbf{r}_j(t_0)]\rangle \quad (6)$$

$$\lambda = \lim_{t\to\infty}\lambda(t) \quad (7)$$

where $\lambda(t)$ is the value of λ calculated for a finite time t, $\langle\rangle$ denotes an ensemble average over possible starting times t_0, e is the charge of an electron, V is the simulation box volume, k_B is Boltzmann's constant, T is temperature, z_i is the charge on ion i in units of electrons, $\mathbf{r}_i(t)$ is the position of ion i at time t, and summation accounts for all N ions in the simulation box (i.e., $N/2$ Li^+ ions and $N/2$ PF_6^- ions). The diagonal ($i = j$) terms in eq 6 represent the theoretical Nernst−Einstein (uncorrelated) conductivity $\lambda_{NE}(t)$, i.e., the ideal conductivity arising only from ion self-diffusion. The off-diagonal terms in eq 6 account for correlated ion motion, which reduces electrolyte conductivity relative to the Nernst−Einstein value.

Figure 3 shows $\lambda_{NE}(t)$ versus time for 1.0 M $LiPF_6$ in EC, DMC, and EC/DMC solvents at 300 and 400 K. Figure 4 shows $\lambda(t)$ for the same systems as in Figure 3. While the curves in Figure 3 at 300 K and the curves in Figure 4 at both 300 and 400 K do not attain steady values within the allotted simulation time, indicating that longer simulations are required to get precise values for conductivity, several trends are nonetheless apparent.

As expected, the Nernst−Einstein conductivities follow the same trends observed for ion diffusivity; that is, conductivity for pure DMC systems is significantly higher than for pure EC systems, with intermediate values for mixed EC/DMC systems. $\lambda_{NE}(t)$ increases significantly as salt concentration is increased from 0.1 M (not shown) to 1.0 M. When Figures 3 and 4 are compared, it is seen that true conductivities are significantly lower (by at least an order of magnitude) than the Nernst−Einstein values. More interestingly, true conductivities for pure EC systems are significantly higher than for pure DMC systems, which is the opposite of the trend for Nernst−Einstein conductivities. More specifically, the steady and consistent downward trend for the DMC curves in Figure 4 suggests conductivity in DMC systems is negligible, in spite of significantly higher diffusivity. Also, unlike the Nernst−Einstein case and consistent with experimental observations,[31,32] conductivities for mixed EC/DMD systems closely match conductivities for pure EC systems, as opposed to taking values approximately equal to the average of the pure EC and pure DMC conductivities. Lastly, conductivity does not appear to change significantly as salt concentration is varied between 0.1 (not shown), 0.3 (not shown), and 1.0 M, but this is difficult to judge due to the short simulation times and poor statistics at low $LiPF_6$ concentration. These observations all suggest conductivity is strongly influenced by correlated ion movement and this correlated movement can vary significantly between solvents.

Ionic conductivities predicted for systems composed of 1.0 M $LiPF_6$ in pure EC or mixed EC/DMC at 300 K appear to be approximately 10% to 20% of experimental values.[31,32] Ionic conductivity for DMC system is under-predicted by an even greater degree.[32] The under-prediction of ionic conductivity from simulation partly results from the previously described under-prediction of diffusivity and likely partly from an over-prediction of correlated ion movement. Use of a more accurate (e.g., polarizable) forcefield could directly reduce ion pairing and correlated motion and could indirectly increase diffusivity by reducing viscosity via reduced formation of molecular clusters and networks.

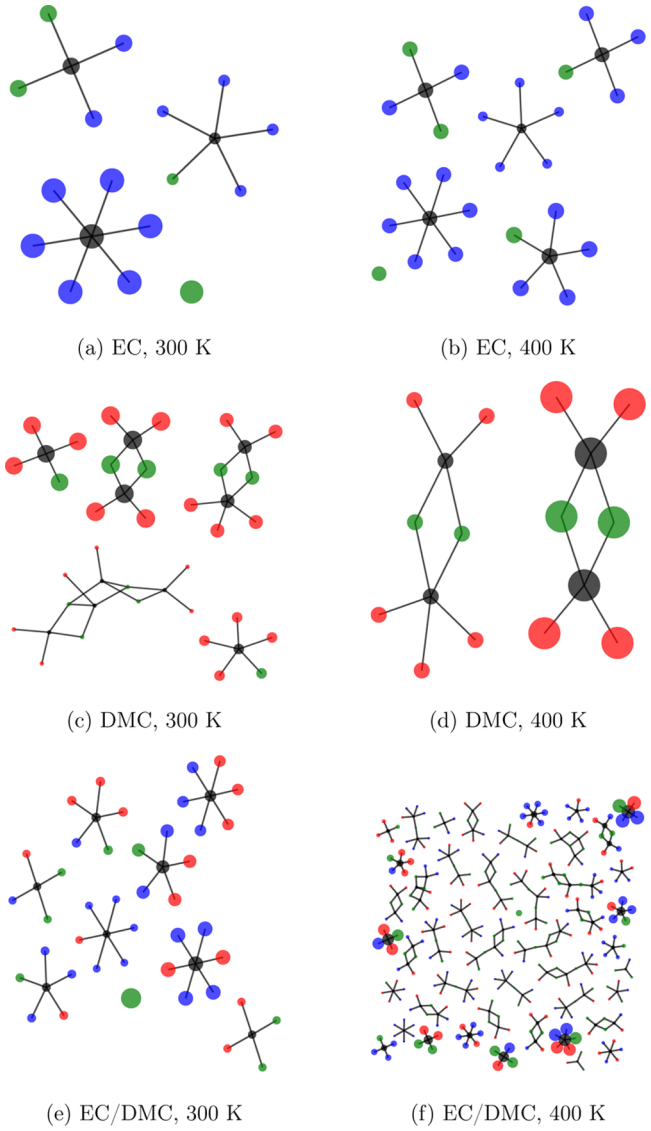

Figure 7. Cluster topologies formed by Li^+ (black), PF_6^- (green), and solvent carbonyl oxygen atoms (EC = blue, DMC = red). Edges (lines) represent neighbor pairing. Node size for a cluster is proportional to the probability of finding an ion in a cluster with that topology. The systems are composed of 0.1 M $LiPF_6$ in EC, DMC, or EC/DMC solvents at 300 and 400 K.

Pair Correlation. Figure 5 shows the pair correlation functions $g(r)$ versus separation r for Li^+ with solvent carbonyl oxygens (Li−O), PF_6^- (Li−P), and other Li^+ (Li−Li) for 1.0 M $LiPF_6$ in EC, DMC, and EC/DMC solvents at 300 and 400 K. The primary Li−O peaks occur at approximately r = 2.1 Å for both EC and DMC in all solvent systems. This compares well with time-of-flight neutron diffraction measurements for $LiPF_6$ in propylene carbonate (PC), which located the primary Li−O peak at 2.04 Å.[10] Primary Li−O peaks calculated from classical and ab initio MD simulations of $LiPF_6$ in EC, DMC, and PC vary from 1.9 to 2.0 Å.[15−17,19,33] Very slight secondary Li−O peaks

dx.doi.org/10.1021/jp4039122 | J. Phys. Chem. C 2013, 117, 24673−24684

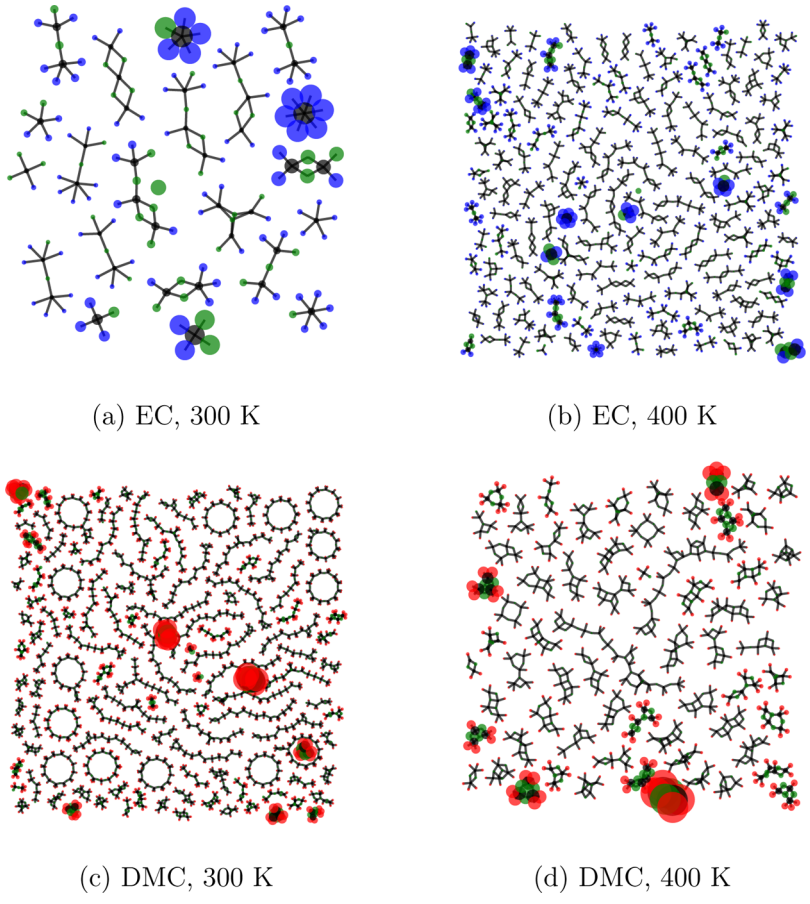

Figure 8. As in Figure 7, except 1.0 M $LiPF_6$ in EC or DMC solvents.

occur at approximately r = 8.1 Å for EC and r = 5.9 Å for DMC. As temperature is increased, the secondary peak for DMC becomes slightly more prominent, and the secondary peaks for both EC and DMC shift to slightly lower values of r. Changes in $LiPF_6$ concentration (not shown) do not appear to significantly change the Li−O $g(r)$ for any solvent/temperature combination.

Similar to the Li−O case, primary Li−P peaks occur at the same distance for all solvent systems, approximately r = 3.2 Å, which agrees with results from classical MD simulations using a polarizable force field for $LiPF_6$ in EC and DMC.[15] Very slight secondary peaks also occur at approximately r = 9.1 Å for EC and r = 6.6 Å for DMC. As temperature is increased, the secondary Li−P peak for EC becomes less prominent and broadens to include a shoulder at approximately r = 7.1 Å, whereas the secondary Li−P peak for DMC becomes more prominent and less broad. Lower $LiPF_6$ concentration (not shown) may increase the prominence of the secondary Li−P peaks for all solvent/temperature combinations, but results are noisy due to poor statistics with the reduced number of Li^+ and PF_6^- species.

The primary Li−Li peaks $g(r)$ in Figure 5 have maxima at approximately r = 4.3 Å and shoulders or subpeaks at approximately r = 5.7 Å for all solvent systems. The primary Li−Li peaks for EC are significantly less prominent than those for DMC, with EC/DMC values being intermediate, which is indicative of reduced ion pairing with increasing EC content. Secondary Li−Li peaks occur at approximately r = 9.2 Å for EC systems but are minor to nonexistent for DMC systems. Increasing temperature greatly increases the prominence of the primary Li−Li peak for EC, decreases prominence of any secondary peak, and reduces shoulders or subpeaks in the primary peak for all solvent systems. Results from lower $LiPF_6$ concentrations (not shown) are inconclusive due to poor statistics with the reduced number of Li^+ species.

Tables 2−4 list the average number of solvent carbonyl oxygen atoms (N_{Li-O}), PF_6^- ions (N_{Li-P}), and Li^+ ions (N_{Li-Li}), respectively, within the first coordination shells of Li^+ ions for all combinations of solvent, temperature, and $LiPF_6$ concentration used in this study. These first shell coordination numbers N_{i-j} are calculated according to

$$N_{i-j} = 4\pi \int_0^{r_{min}} r^2 g_{i-j}(r) \rho_j \, dr \tag{8}$$

where ρ_j is the average number density of species j and r_{min} is the location of the minimum after the first peak in the corresponding pair correlation function $g_{i-j}(r)$ (e.g., from Figure 5 r_{min} is approximately 3.3 Å for Li−O interactions, 4.5 Å for Li−P interactions, and 6.8 Å for Li−Li interactions).

N_{Li-O} decreases for all solvent systems as either temperature or $LiPF_6$ concentration is increased, with EC coordination being the most sensitive. N_{Li-O} for EC systems varies from 2.9 (1.0 M, 400 K) to 5.2 (0.1 M, 300 K) and for DMC systems from 2.0 (1.0 M, 400 K) to 2.6 (0.1 M, 300 K). Results for mixed EC/DMC systems take on intermediate values, with N_{Li-O} for EC molecules always at least slightly greater than N_{Li-O} for DMC molecules.

This behavior is driven by the larger molecular dipole (and relative value of dielectric constant) of EC compared to DMC. In addition, the compact geometry of the cyclic EC molecule lends itself to a more efficient packing and coordiantion to Li^+ compared to the linear and open structure of DMC molecules.

dx.doi.org/10.1021/jp4039122 | J. Phys. Chem. C 2013, 117, 24673−24684

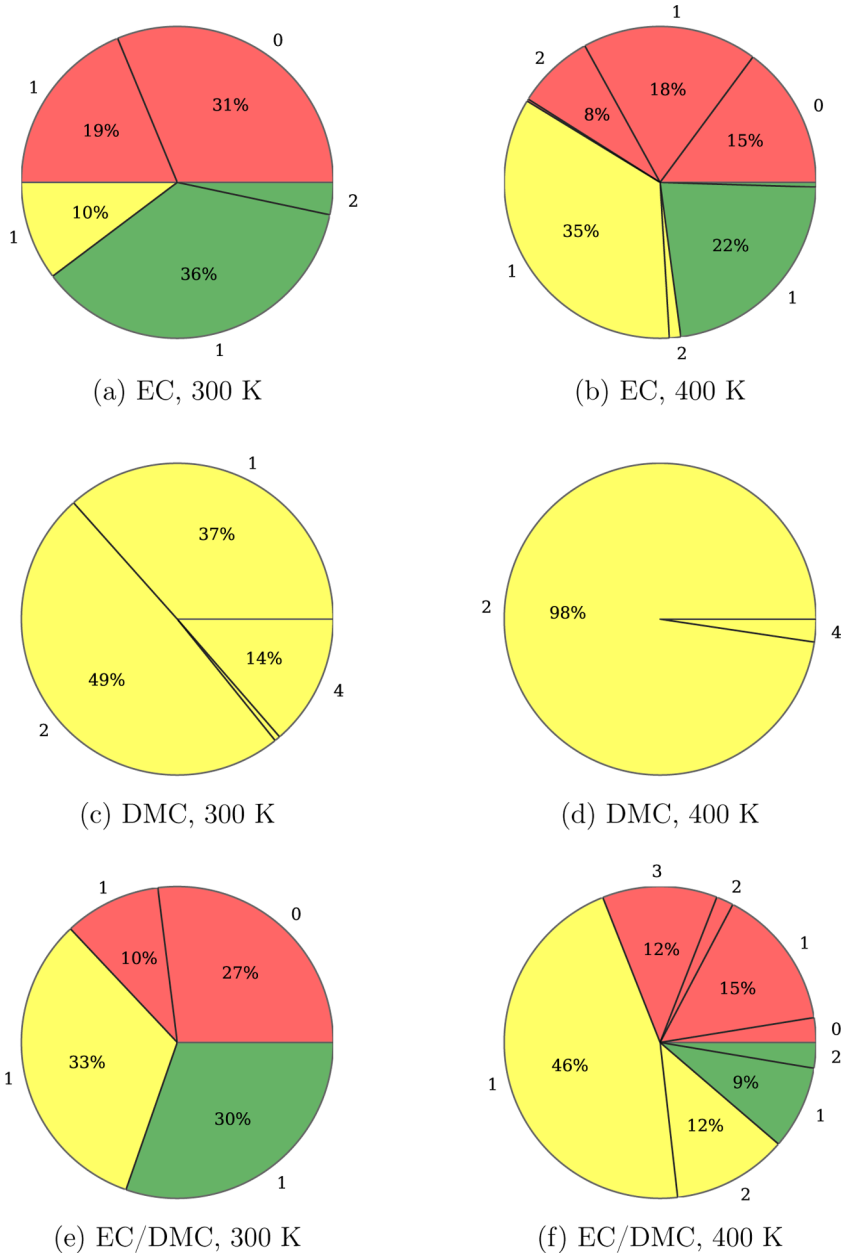

Figure 9. Probability of finding an ion within a cluster of particular charge (red = −1, yellow = 0, and green = +1) and containing a particular number of Li^+ (numbers around chart perimeter). Systems are composed of 0.1 M $LiPF_6$ in EC, DMC, or EC/DMC solvent at 300 or 400 K.

Compared to DMC, the coordination numbers for EC carbonyl oxygens about Li^+ are larger for all salt concentrations and temperatures, including those for EC/DMC systems where there is direct competition of both solvent molecules for Li^+.

For comparison, results from ab initio MD simulations of 0.5 M $LiPF_6$ in EC at 310 and 400 K predicted $N_{Li-O} \approx 4$.[19] Better matching the range of N_{Li-O} values found in the current study, classical MD simulations using a polarizable force field for approximately 1.0 M $LiPF_6$ at 298 K (363 K) predicted N_{Li-O} values of 3.6 (3.3) in pure EC and 2.7 (2.4) in pure DMC.[15] Contrary to the current findings, which predict slightly greater association of EC with Li^+ relative to DMC (i.e., EC/dmc versus ec/DMC in Table 2), Borodin and Smith predict slightly greater association for DMC; but the total number of associating solvent molecules around Li^+ is similar at ~3.[15]

N_{Li-P} trends are generally opposite those for N_{Li-O}. N_{Li-P} increases for all solvent systems as either temperature or $LiPF_6$ concentration is increased, with EC coordination still being the most sensitive. This reversal of trends suggests solvent carbonyl oxygen atoms and PF_6^- compete for coordination with Li^+. N_{Li-P} for EC systems varies from 0.4 (0.1 M, 300 K) to 1.6 (1.0 M, 400 K) and for DMC systems from 1.7 (0.1 M, 300 K) to 2.2 (1.0 M, 400 K). Results for mixed EC/DMC systems again take on intermediate values, generally closer to the pure EC results. Classical MD simulations using a polarizable force field predicted N_{Li-P} values approximately 0.5 lower than the results in this work, which indicates reduced ion pairing; but trends in N_{Li-P} with variations in temperature and solvent are in good agreement.[15]

N_{Li-Li} trends generally match those for N_{Li-P}, suggesting that association of Li^+ with other Li^+ may depend upon PF_6^- as an intermediary. N_{Li-Li} for EC systems varies from 0.0 (0.1 M, 300 K) to 0.9 (1.0 M, 400 K) and for DMC systems from 0.9 (0.1 M, 300 K) to 1.7 (1.0 M, 400 K), suggesting that formation

dx.doi.org/10.1021/jp4039122 | J. Phys. Chem. C 2013, 117, 24673−24684

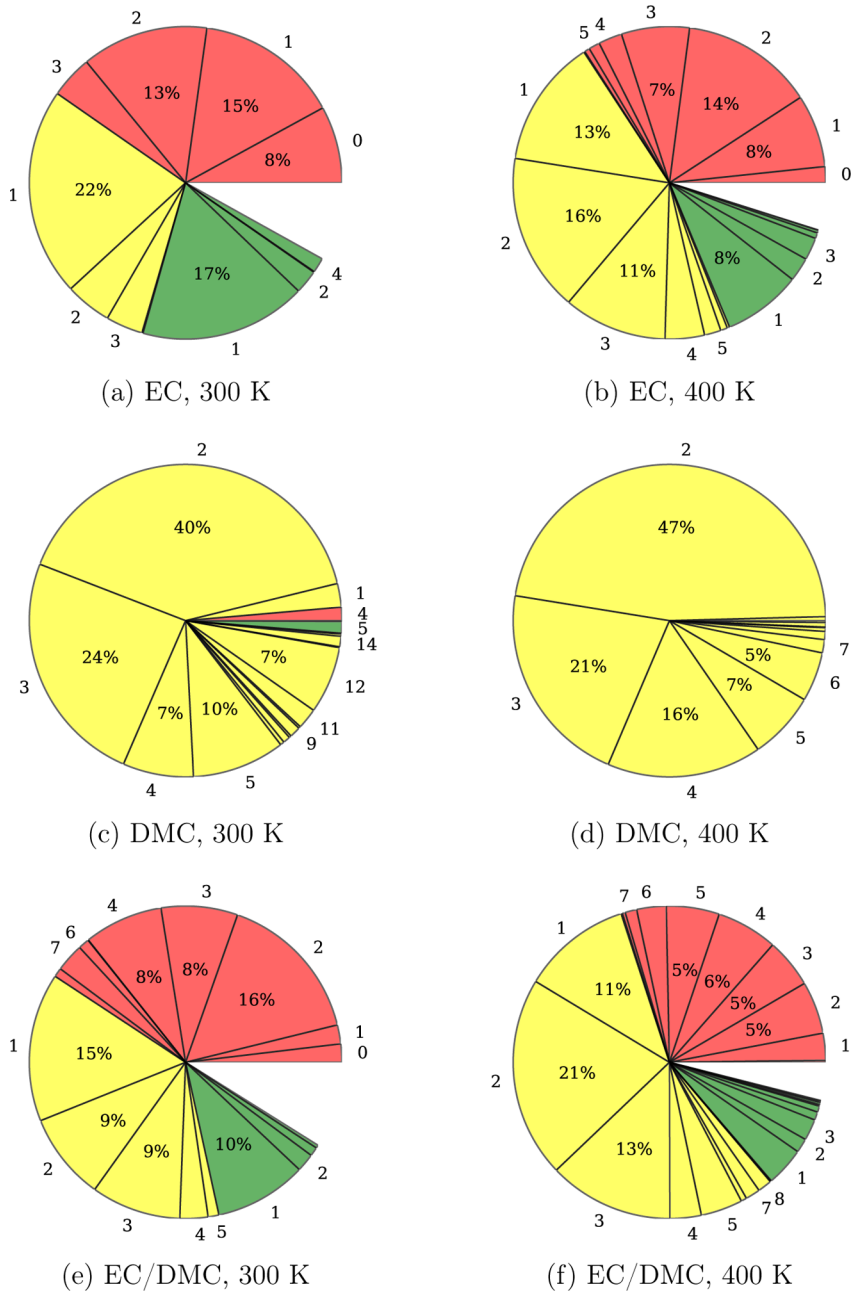

Figure 10. As in Figure 9, except 1.0 M $LiPF_6$. An incomplete pie chart indicates cluster charges other than −1, 0, or +1.

of clusters containing multiple Li^+ is the norm for DMC systems and less extensive for EC systems. This will be shown explicitly via cluster analysis later in this paper. Results for mixed EC/DMC systems are again intermediate and closer to EC results, particularly at low $LiPF_6$ concentration.

For any given time step, if a particular PF_6^- or Li^+ ion is within the first coordination shell of a particular Li^+ ion, those ions will be referred to as "neighbors". Similarly, if a particular solvent carbonyl oxygen atom is within the first coordination shell of a particular Li^+ ion, that solvent molecule and that Li^+ are neighbors. (Other solvent atoms are ignored for the purpose of neighbor determination, because their association with Li^+ is negligible compared to the carbonyl oxygen, which is consistent with findings from quantum density functional theory calculations of interactions between Li^+ and EC.[34]) An adjacency matrix $A(\tau)$ is formed wherein $A_{i,j}(\tau) = 1$ if object i (e.g., one of the Li^+ ions) and object j (e.g., one of the PF_6^- ions) are neighbors at time τ and 0 otherwise. The neighbor autocorrelation function $R(t)$ is the probability that a particular neighbor pair at time t_0 will also be neighbors at $t_0 + t$. $R(t)$ is calculated according to

$$R(r) = \langle A_{i,j}(t_0) A_{i,j}(t_0 + t) \rangle \tag{9}$$

where $\langle\rangle$ denotes an ensemble average over all possible initial times t_0 and indices i and j.

Figure 6 shows $R(t)$ versus time for coordination of Li^+ with solvent carbonyl oxygens (Li−O), PF_6^- (Li−P), and other Li^+ (Li−Li) for 1.0 M $LiPF_6$ in EC, DMC, and EC/DMC solvents at 300 and 400 K. The $R(t)$ curves for Li−O indicate that Li^+ ions tend to swap solvent neighbors within a few nanoseconds at 300 K and within a nanosecond at 400 K. Reducing $LiPF_6$ concentration does not appear to significantly influence

dx.doi.org/10.1021/jp4039122 | J. Phys. Chem. C 2013, 117, 24673−24684

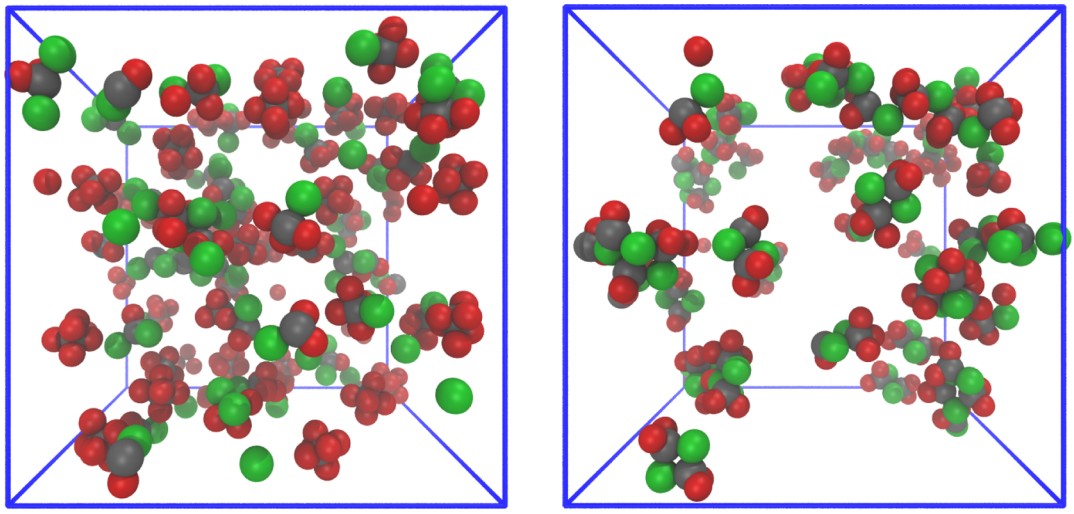

Figure 11. Trajectory snapshots showing all Li^+ (gray), all P atoms (green) from PF_6^-, and only solvent carbonyl oxygen atoms (red) neighbored with a Li^+. The systems are 1.0 M $LiPF_6$ in pure EC and DMC at 300 K. The blue box outlines the periodic simulation cell. Note that some clusters may span periodic boundaries.

characteristic times for Li−O pairing (not shown). The characteristic times for Li−P pairing are longer than the 20 ns simulation time at 300 K and are approximately 5 to 15 ns at 400 K. Characteristic times for Li−Li pairing are much longer than Li−O values and appear to be approximately half the Li−P values, which is consistent with Li−Li association occurring through PF_6^- intermediates. Characteristic times for Li−P and Li−Li pairing appear to be significantly reduced for systems containing EC solvent. Trends in Li−P and Li−Li pairing for lower $LiPF_6$ concentration are not discernible due to poor statistics.

Molecular Clustering. Within graph theory a "graph" is a collection of "nodes" or "vertices", pairs of which may be connected by "edges". For any given time step τ, a graph can be constructed in which the nodes represent specific Li^+ ions, PF_6^- ions, or solvent carbonyl oxygen atoms and edges connect specific Li−O and Li−P neighbor pairs (as defined above). For this discussion we define a cluster as a connected component of such a graph, i.e a subgraph in which every node is connected to every other node in the subgraph by at least one path and is not connected to any node not in the subgraph. For every time step there will then exist a set of clusters with a variety of network topologies or patterns of connectedness. Clusters are isomorphic and counted as equivalent if they have the same network of bonds connecting the same set of atom types. Cluster analysis was aided by the open source Python package NetworkX v1.7.[35] Graph theory has also been used to study hydrogen-bonded networks around aqueous solutes.[36]

Figures 7 and 8 show cluster topologies formed by Li^+, PF_6^-, and solvent carbonyl oxygen atoms. For clarity, up to 15% of the least likely cluster topologies are omitted. (1.0 M EC/DMC systems are not presented, because the number of minor topologies becomes too numerous to display clearly.) Figures 9 and 10 show more quantitatively the probability of finding an ion within a cluster of a particular charge and number of Li^+.

Figure 7a shows that the most common cluster topology for 0.1 M $LiPF_6$ EC systems at 300 K is a single Li^+ surrounded by six EC molecules, resulting in a cluster with +1 charge. A single un-neighbored PF_6^- (a lone green node) is approximately as common. Increasing temperature and/or $LiPF_6$ concentration (Figures 7b and 8a,b) generally results in a greater variety of cluster topologies for EC systems, but dissociated Li^+ and PF_6^- remain similar. Figures 9a,b and 10a,b clearly show that the likelihood of forming neutral clusters (yellow) increases with both temperature and $LiPF_6$ concentration. This increased formation of clusters with zero charge may offset gains in conductivity expected with increased temperature and salt concentration. The extent of this effect will be influenced by the characteristic lifetime of individual clusters; but given the relatively long correlation time for neighboring between Li^+ and PF_6^- (Figure 6), this effect is likely non-negligible. Further, while clusters with +1 charge (green) are almost always built around a single Li^+, the number of Li^+ in clusters with −1 charge (red) or 0 charge varies significantly, with more Li^+ being more likely at higher temperature and $LiPF_6$ concentration. This binding of multiple Li^+ into larger clusters should also reduce conductivity, relative to the ideal case of complete dissociation. All bridging of Li^+ occurs via intermediate PF_6^- anions. Solvent carbonyl oxygens were not observed simultaneously neighboring with multiple Li^+. Averaging over all observed clusters for a particular system, the average number of solvent molecules and PF_6^- ions neighbored with Li^+ equals the coordination numbers listed in Tables 2 and 3, respectively. Note, however, that the most common cluster topology does not match the coordination implied by the results in Tables 2 and 3. Figure 11a is a simulation snapshot showing clusters formed in the system composed of 1.0 M $LiPF_6$ in pure EC at 300 K. The common topology of Li^+ surrounded by six solvent molecules is readily apparent.

For DMC systems the dominant cluster topology is two Li^+ ions, each neighbored with two or three different solvent molecules and connected to each other via two shared PF_6^- neighbors (Figures 7c,d and 8c,d). At 300 K clusters composed of a single Li^+, a single PF_6^-, and three or four solvent molecules are also likely (Figure 7c). Increasing $LiPF_6$ concentration leads to increased cluster variety, but unlike EC systems, the vast majority of clusters observed in DMC systems have zero charge, which is clearly seen in Figures 9c,d and 10c,d. Given the relatively long correlation time for neighboring between Li^+ and PF_6^-,

dx.doi.org/10.1021/jp4039122 | J. Phys. Chem. C 2013, 117, 24673−24684

particularly for DMC systems, the formation of primarily neutral clusters is consistent with the negligible ionic conductivity observed for DMC systems (Figure 4). Also unlike EC systems, decreasing temperature generally results in a reduced variety of cluster topologies. Relative to EC systems, the formation of extended chains or rings is much more likely in DMC systems. In clusters containing more than one Li^+, the Li^+ associate with each other via one to three (typically two) intermediate PF_6^-. Solvent carbonyl oxygens were not observed simultaneously neighboring with multiple Li^+. Figure 11a is a simulation snapshot showing clusters formed in the system composed of 1.0 M $LiPF_6$ in pure DMC at 300 K. Relative to the EC system shown in Figure 11a, there are fewer and larger clusters in the DMC system.

Due to the presence of two solvent types, a wider variety of cluster topologies is observed for EC/DMC systems (Figure 7e,f). The general pattern of topologies, however, is more similar to EC systems than DMC systems, with reduced formation of extended chains or rings and fewer neutral clusters. This observation is consistent with ionic conductivity for EC/DMC systems more closely matching EC systems than DMC systems (Figure 4). Although the EC-like topology of a single Li^+ surrounded by several solvent molecules in a cluster with +1 charge is still prevalent in EC/DMC systems, many of the typical EC positions in the structure are replaced by DMC. Non-neutral clusters in both EC and EC/DMC systems are more likely to have charges of −1 than +1, with this trend being stronger in EC/DMC systems and at higher temperature (Figures 9 and 10).

SUMMARY

Classical molecular dynamics (MD) simulations were used to examine structure and transport properties of nonaqueous lithium-ion electrolytes composed of $LiPF_6$ dissolved in either pure ethylene carbonate (EC), pure dimethylene carbonate (DMC), or a 1:1 EC/DMC mixture. Diffusivities and ionic conductivities were calculated from MD trajectories for each of the three solvent systems at multiple temperatures and $LiPF_6$ concentrations. Contrary to Nernst−Einstein theory, pure DMC systems had the greatest diffusivity but the lowest conductivity. Conventional pair distribution and graph theoretic tools were then used to describe ion and solvent clustering in each system. Consistent with the low ionic conductance of systems using pure DMC as solvent, most ion clusters in DMC systems had zero net charge. Conversely, EC and EC/DMC systems, which were conductive, contained numerous clusters with net +1 or −1 charge. The differences in clustering behavior for EC and DMC systems are explained by their very different dielectric constants.

Bulk electrolyte diffusivity and nanoscale ion clustering can both significantly influence ionic conductivity. The ideal solvent must associate strongly enough with individual cations and/or anions to minimize their pairing, without being overly viscous. In the case of EC/DMC blends used in commercial lithium-ion batteries, a compromise is reached, wherein the highly dielectric EC inhibits cation and anion association and DMC allows sufficient fluidity and diffusion.

ASSOCIATED CONTENT

Supporting Information

Simulation force field parameters and example input scripts. This material is available free of charge via the Internet at http://pubs.acs.org.

AUTHOR INFORMATION

Corresponding Author

*E-mail: cmtenne@sandia.gov. Phone: (505) 284-4466. Fax: (505) 844-7354.

Notes

The authors declare no competing financial interest.

ACKNOWLEDGMENTS

Sandia National Laboratories is a multiprogram laboratory managed and operated by Sandia Corporation, a wholly owned subsidiary of Lockheed Martin Corporation, for the U.S. Department of Energy's National Nuclear Security Administration under Contract DE-AC04-94AL85000. This work was supported by the Laboratory Directed Research and Development program of Sandia National Laboratories.

REFERENCES

(1) Armand, M.; Tarascon, J. M. Building Better Batteries. *Nature* **2008**, *451*, 652−657.
(2) Goodenough, J. B.; Kim, Y. Challenges for Rechargeable Li Batteries. *Chem. Mater.* **2010**, *22*, 587−603.
(3) Xu, K. Nonaqueous Liquid Electrolytes for Lithium-Based Rechargeable Batteries. *Chem. Rev.* **2004**, *104*, 4303−4417.
(4) Smart, M. C.; Ratnakumar, B. V.; Surampudi, S. Electrolytes for Low-Temperature Lithium Batteries Based on Ternary Mixtures of Aliphatic Carbonates. *J. Electrochem. Soc.* **1999**, *146*, 486−492.
(5) Burba, C. M.; Frech, R. Spectroscopic Measurements of Ionic Association in Solutions of $LiPF_6$. *J. Phys. Chem. B* **2005**, *109*, 15161−15164.
(6) Kurisaki, T.; Tanaka, D.; Inoue, Y.; Wakita, H.; Minofar, B.; Fukuda, S.; Ishiguro, S.-i.; Umebayashi, Y. Surface Analysis of Ionic Liquids with and Without Lithium Salt Using X-Ray Photoelectron Spectroscopy. *J. Phys. Chem. B* **2012**, *116*, 10870−10875.
(7) Maerkle, W.; Colin, J.-F.; Goers, D.; Spahr, M. E.; Novak, P. In Situ X-Ray Diffraction Study of Different Graphites in a Propylene Carbonate Based Electrolyte at Very Positive Potentials. *Electrochim. Acta* **2010**, *55*, 4964−4969.
(8) Soetens, J. C.; Millot, C.; Maigret, B.; Bako, I. Molecular Dynamics Simulation and X-Ray Diffraction Studies of Ethylene Carbonate, Propylene Carbonate and Dimethyl Carbonate in Liquid Phase. *J. Mol. Liq.* **2001**, *92*, 201−216.
(9) Yang, L.; Xiao, A.; Lucht, B. L. Investigation of Solvation in Lithium Ion Battery Electrolytes by NMR Spectroscopy. *J. Mol. Liq.* **2010**, *154*, 131−133.
(10) Kameda, Y.; Umebayashi, Y.; Takeuchi, M.; Wahab, M. A.; Fukuda, S.; Ishiguro, S. I.; Sasaki, M.; Amo, Y.; Usuki, T. Solvation Structure of Li^+ in Concentrated $LiPF_6$-Propylene Carbonate Solutions. *J. Phys. Chem. B* **2007**, *111*, 6104−6109.
(11) Halls, M. D.; Tasaki, K. High-Throughput Quantum Chemistry and Virtual Screening for Lithium Ion Battery Electrolyte Additives. *J. Power Sources* **2010**, *195*, 1472−8.
(12) Selvam, P.; Tsuboi, H.; Koyama, M.; Endou, A.; Takaba, H.; Kubo, M.; Del Carpio, C. A.; Miyamoto, A. Computational Chemistry for Industrial Innovation. *Rev. Chem. Eng.* **2006**, *22*, 377−470.
(13) Hamad, I. A.; Novotny, M. A.; Wipf, D. O.; Rikvold, P. A. A New Battery-Charging Method Suggested by Molecular Dynamics Simulations. *Phys. Chem. Chem. Phys.* **2010**, *12*, 2740−3.
(14) Borodin, O.; Smith, G. D. LiTFSI Structure and Transport in Ethylene Carbonate from Molecular Dynamics Simulations. *J. Phys. Chem. B* **2006**, *110*, 4971−4977.
(15) Borodin, O.; Smith, G. D. Quantum Chemistry and Molecular Dynamics Simulation Study of Dimethyl Carbonate: Ethylene Carbonate Electrolytes Doped with $LiPF_6$. *J. Phys. Chem. B* **2009**, *113*, 1763−1776.
(16) Takeuchi, M.; Matubayasi, N.; Kameda, Y.; Minofar, B.; Ishiguro, S.; Umebayashi, Y. Free-Energy and Structural Analysis of Ion Solvation

and Contact Ion-Pair Formation of Li^+ with BF4- and PF6- in Water and Carbonate Solvents. *J. Phys. Chem. B* **2012**, *116*, 6476−6487.
(17) Yu, J. M.; Balbuena, P. B.; Budzien, J.; Leung, K. Hybrid DFT Functional-Based Static and Molecular Dynamics Studies of Excess Electron in Liquid Ethylene Carbonate. *J. Electrochem. Soc.* **2011**, *158*, A400−A410.
(18) Bhatt, M. D.; Cho, M.; Cho, K. Density Functional Theory Calculations and Ab Initio Molecular Dynamics Simulations for Diffusion of Li^+ Within Liquid Ethylene Carbonate. *Modell. Simul. Mater. Sci. Eng.* **2012**, *20*, 065004.
(19) Ganesh, P.; Jiang, D. E.; Kent, P. R. C. Accurate Static and Dynamic Properties of Liquid Electrolytes for Li-Ion Batteries from Ab Initio Molecular Dynamics. *J. Phys. Chem. B* **2011**, *115*, 3085−3090.
(20) Vorobyov, I.; Anisimov, V. M.; Greene, S.; Venable, R. M.; Moser, A.; Pastor, R. W.; MacKerell, A. D. Additive and Classical Drude Polarizable Force Fields for Linear and Cyclic Ethers. *J. Chem. Theory Comput.* **2007**, *3*, 1120−1133.
(21) Jensen, K. P.; Jorgensen, W. L. Halide, Ammonium, and Alkali Metal Ion Parameters for Modeling Aqueous Solutions. *J. Chem. Theory Comput.* **2006**, *2*, 1499−1509.
(22) Frisch, M. J. et al. *Gaussian 03*, revision C.02; Gaussian Inc.: Wallingford, CT, 2004.
(23) Wang, J.; Wang, W.; Kollman, P.; Case, D. Automatic Atom Type and Bond Type Perception in Molecular Mechanical Calculations. *J. Mol. Graph. Model.* **2006**, *25*, 247−260.
(24) Wang, J.; Wolf, R. M.; Caldwell, J. W.; Kollman, P. A.; Case, D. A. Development and Testing of a General Amber Force Field. *J. Comput. Chem.* **2004**, *25*, 1157−1174.
(25) Bayly, C. I.; Cieplak, P.; Cornell, W.; Kollman, P. A. A Well-Behaved Electrostatic Potential Based Method Using Charge Restraints for Deriving Atomic Charges: The RESP Model. *J. Phys. Chem.* **1993**, *97*, 10269−10280.
(26) Cieplak, P.; Cornell, W. D.; Bayly, C.; Kollman, P. A. Application of the Multimolecule and Multiconformational RESP Methodology to Biopolymers: Charge Derivation for DNA, RNA, and Proteins. *J. Comput. Chem.* **1995**, *16*, 1357−1377.
(27) Plimpton, S. J. Fast Parallel Algorithms for Short-Range Molecular Dynamics. *J. Comput. Phys.* **1995**, *117*, 1−19.
(28) Plimpton, S. J. *LAMMPS Molecular Dynamics Simulator*. http://lammps.sandia.gov.
(29) Martínez, L.; Andrade, R.; Birgin, E. G.; Martínez, J. M. PACKMOL: A Package for Building Initial Configurations for Molecular Dynamics Simulations. *J. Comput. Chem.* **2009**, *30*, 2157−2164.
(30) Hayamizu, K.; Aihara, Y.; Arai, S.; Martinez, C. G. Pulse-Gradient Spin-Echo H-1, Li-7, and F-19 NMR Diffusion and Ionic Conductivity Measurements of 14 Organic Electrolytes Containing $LiN(SO_2CF_3)(2)$. *J. Phys. Chem. B* **1999**, *103*, 519−524.
(31) Hayamizu, K. Temperature Dependence of Self-Diffusion Coefficients of Ions and Solvents in Ethylene Carbonate, Propylene Carbonate, and Diethyl Carbonate Single Solutions and Ethylene Carbonate Plus Diethyl Carbonate Binary Solutions of $LiPF_6$ Studied by NMR. *J. Chem. Eng. Data* **2012**, *57*, 2012−2017.
(32) Hayashi, K.; Nemoto, Y.; Tobishima, S.; Yamaki, J. Electrolyte for High Voltage $Li/LiMn_{1.9}Co_{0.1}O_4$ Cells. *J. Power Sources* **1997**, *68*, 316−319.
(33) Li, T.; Balbuena, P. B. Theoretical Studies of Lithium Perchlorate in Ethylene Carbonate, Propylene Carbonate, and Their Mixtures. *J. Electrochem. Soc.* **1999**, *146*, 3613−3622.
(34) Bhatt, M. D.; Cho, M.; Cho, K. Interaction of Li^+ Ions with Ethylene Carbonate (EC): Density Functional Theory Calculations. *Appl. Surf. Sci.* **2010**, *257*, 1463−1468.
(35) Hagberg, A. A.; Schult, D. A.; Swart, P. J. Exploring Network Structure, Dynamics, and Function Using NetworkX. Proceedings of the 7th Python in Science Conference (SciPy2008). Pasadena, CA, 2008; pp 11−15.
(36) Mooney, B. L.; Corrales, L. R.; Clark, A. E. MoleculaRnetworks: An Integrated Graph Theoretic and Data Mining Tool to Explore Solvent Organization in Molecular Simulation. *J. Comput. Chem.* **2012**, *33*, 853−860.